First Experimental Results for a WiFi-Based Passive Forward Scatter Radar

T. Martelli, F. Colone, P. Lombardo

DIET Dept., University of Rome "La Sapienza"
Via Eudossiana, 18 – 00184 Rome, Italy
e-mail: {martelli, colone, lombardo}@diet.uniroma1.it

***Abstract*—In this paper we investigate the potentiality to exploit a passive forward scatter radar (PFSR) based on WiFi transmissions for vehicle classification. In particular, a procedure to extract the vehicle signatures from the received signal is presented. The preliminary results obtained by means of an experimental setup developed and fielded at University of Rome "La Sapienza" show that different targets yield quite different signature shapes that can be fruitfully exploited by a classification stage according to a reasonable strategy.**

Keywords—Forward scatter radar, passive radar, WiFi transmissions, vehicle classification.

I. INTRODUCTION

In the last years, the forward scattering radar (FSR) has received significantly interest. FSR is an extreme bistatic radar configuration where the bistatic angle is near to 180°, [1]-[2]. Differently from monostatic and bistatic operation modes, the received signal is not the reflection from the target but rather the shadow of the target. In fact, when the target moves on or close to the baseline, it blocks part of the transmitted signal and this leads to a reduction of the received signal power.

As well known in the literature, the FSR offers a number of interesting features such as simple hardware required for implementation and an enhanced target radar cross-section compared to conventional operation mode. Moreover, the received forward scattering signal is independent from the target material, which means that FSR is robust to stealth technology. On the other hand, it is characterized by the absence of range resolution and a limited operation area.

Numerous works proved the effectiveness of FSR using active systems. For example, in [3]-[4] it was shown that FSR can be used for ground target detection and classification. In [5]-[6] FSR is applied for air target detection and tracking whereas in [7] for detection and classification of maritime objects. Moreover, recently, there has been a growing attention in the use of FSR configuration in passive radar (PR) [8]. In fact, the exploitation of an existing illuminator of opportunity allows additional advantages such as low cost, low vulnerability to electronic countermeasure, covert operation and low environmental impact. In particular, in [9]-[12] has been demonstrated the feasibility of such geometry using GSM, GNSS and DVB-T signals as illuminators of opportunity.

Aiming at local area monitoring, WiFi transmissions have been exploited for target detection, localization and imaging against conventional geometries [13]-[15], since they offer reasonable bandwidth (range resolution), coverage and wide accessibility. In this work, WiFi signals are considered as potential source of opportunity for a passive radar in forward scatter configuration. In particular, we investigated the potentialities of WiFi-based PFSR for Automatic Target Classification (ATC) of ground moving targets.

A proper processing scheme able to extract the vehicle signatures from the received signal is proposed. Then, a target classification approach based on minimum Euclidean distance criteria has been presented. In order to preliminary verify the effectiveness of the proposed system, experimental campaigns have been performed in a wide parking area using different car models as cooperative targets. Preliminary results against the collected data set show that the different targets yield different signature shapes. Consequently, the proposed classification system is able to correctly associate a vehicle signature to its car model. This contributes to prove that the WiFi-based PFSR can be used for barrier coverage applications for its ability to detect and potentially classify ground moving targets within the monitored region.

The paper is organized as follows. The WiFi-based PFSR system is briefly described in Section II. Section III reports the experimental setup used to perform the tests and the acquisition campaign. The comparison of the obtained signatures is shown in Section IV whereas the preliminary results in terms of classification capability are reported in Section V. Finally, our conclusions are drawn in Section VI.

II. WIFI-BASED PASSIVE FSR CONCEPT

Figure 1 show the considered PFSR system. In particular, a WiFi access point (AP), used to provide coverage for an assigned area, is the transmitter of opportunity (TX). The target moves along its trajectory with velocity v and crosses the baseline, i.e. the line joining the TX and the receiver (RX), yielding a bistatic angle $\beta \approx 170°\text{-}180°$.

The main receiving channel (known as surveillance channel) is used to collect the signal received from the observed scene while an additional receiving channel (known as the reference channel) is adopted to collect the transmitted signal that is not known at the receiver. In the considered scenarios, being the sensor typically installed very close to the WiFi AP, we assume the TX to be partially cooperative; therefore, its signal can be spilled from the TX antenna path using a directional coupler. Since the transmitted waveform is not within the control of the radar designer, high sidelobes or undesired peaks appear in the corresponding Ambiguity Function (AF). Therefore, the reference signal must undergo a modulation-dependent conditioning stage aimed at improving the resulting mismatched AF in the range dimension [13]. Then, in order to increase the signal to noise ratio (SNR), the signal collected at the reference channel is used to perform a range compression with the surveillance signal. We recall that WiFi transmissions are of a pulsed type so that the range compression might be obtained by cross-correlating the surveillance and the reference signals on a pulse basis.

From the range compressed data, the slow-time profile at the direct signal range bin is obtained. Subsequently, its square modulus is extracted, representing the target signature. This can be exploited by a "Signature analysis" block as described in the following sections.

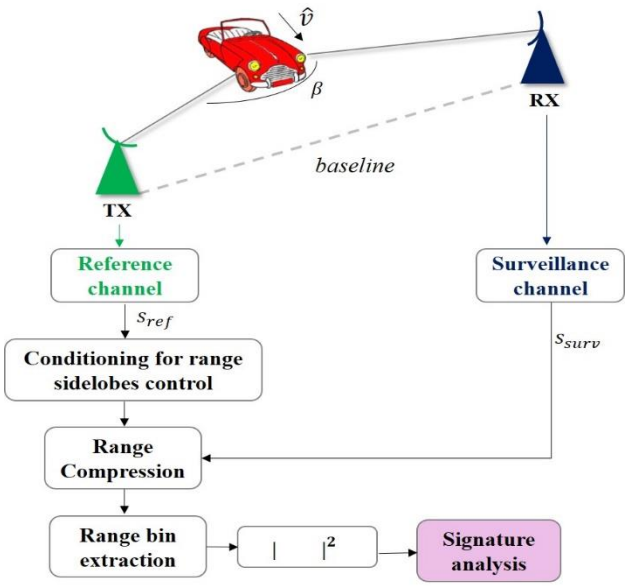

Fig. 1. WiFi-based PFSR system.

III. Acquisitioin Campaign and Data Collection

Aiming at understanding the impact of the forward geometry for applications of vehicles monitoring, a dedicated acquisition campaign has been performed. Specifically, the tests have been performed in a wide parking area in Cisterna di Latina (Italy) and the exploited geometry is depicted in Figure 2. The considered live data have been collected by means of the PR receiver developed at DIET Department of the University of Rome "La Sapienza" (see picture on the upper right corner of Figure 2).

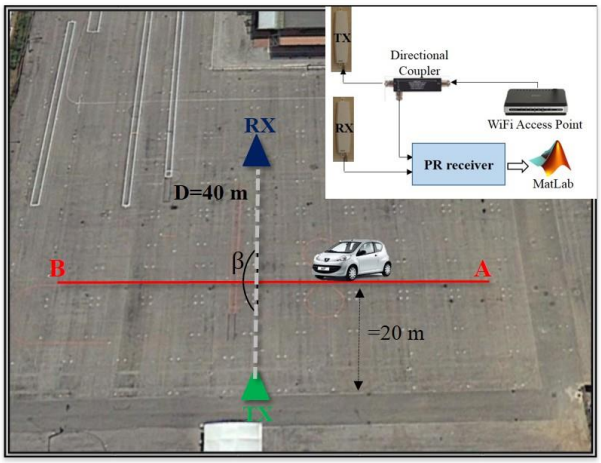

Fig. 2. Sketch of the acquisition geometry.

TABLE I. CAR MODELS USED IN THE ACQUISITION CAMPAIGN.

Car model	Dimensions (length, width, height)	Number of tests
Peugeot 107	3.43 x 1.63 x 1.47 m	8
Volkswagen Polo	3.715 x 1.655 x 1.420 m	4
Citroen C3	3.941 x 1.728 x 1.524 m	5
Fiat Punto Evo	4.065 x 1.690 x 1.49 m	10

A commercial WiFi AP was used as transmitter of opportunity; in particular, it was configured to transmit in channel 6 of the WiFi band (2437 MHz), set up to emit a regular Beacon signal exploiting a DSSS modulation at 3 ms. Its output was connected to the transmitting antenna (TX), located at the point with coordinates (x_{TX}, y_{TX}) = (0,0) m. Then a directional coupler was used to send a -20 dB copy of the transmitted signal (the reference signal) to the first receiving channel. The second channel of the receiving system was directly connected to the surveillance antenna (RX) which was located in (x_{RX}, y_{RX}) = (0,D) m in forward configuration with respect to the TX with baseline D=40 m. Both antennas were mounted at about 1.25 m of height with respect to the ground. After a fully coherent base-band down-conversion stage, the signals collected at the different receiving channels are sampled at 22 MHz and stored for off-line processing.

Different tests have been performed using cars as cooperative targets. The cars move orthogonally to the TX-RX baseline crossing it at the middle point with a bistatic angle $\beta \approx 180°$. Specifically, they move from point A≈(-40,20) m to point B≈(40,20) m (red line in Figure 2) with velocity of about 4-5 m/s depending on the considered test. Four car models have been taken in account: Peugeot 107, Volkswagen Polo, Citroen C3 and Fiat Punto Evo. The dimensions and the number of the performed tests with each car are reported in Table I. Note that, although a limited data set has been considered, cars of similar dimensions have been used (such as Citroen C3 and Punto Evo). The acquisition time of each test is about 20 s.

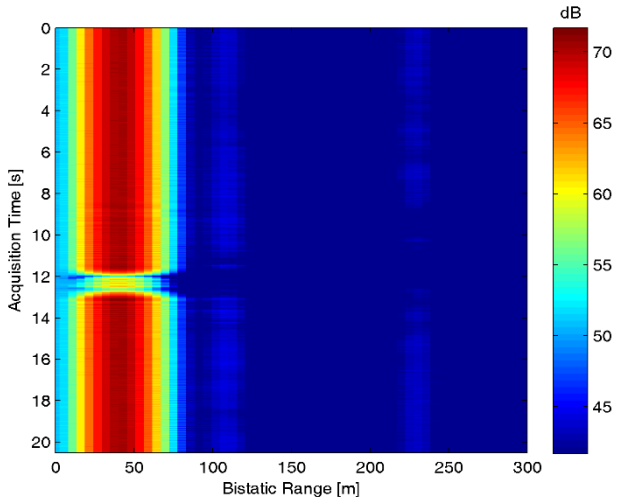

(a)

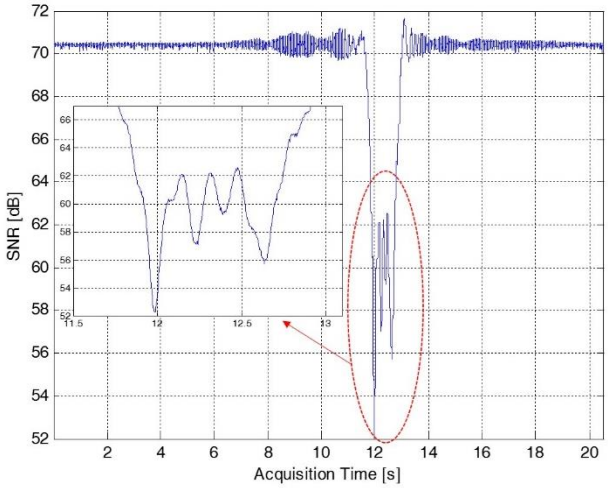

(b)

Fig 3. Results for a Fiat Punto Evo as cooperative target. (a) Bistatic Range- Acquisition time map; (b) Target signature.

The WiFi-based PFSR processing scheme depicted in Figure 1 has been applied against the collected surveillance signal. As an example, Figure 3(a) shows the bistatic range-acquisition time map with range sidelobes control for a test with a Fiat Punto Evo as cooperative target. The map has been normalized to the thermal noise power level so that the value at each map location represents the estimated SNR.

As it is apparent, a strong contribution appears at about 40 m spreading along the acquisition time corresponding to the direct signal transmitted by the transmitting antenna. However, we note a reduction of the direct signal power approximately in correspondence of the time interval form 12 to 13 s; this is a consequence of the fact that when the target crosses the baseline, it blocks the incident wave of the TX antenna. As an example, Figure 3(b) shows the Fiat Punto Evo vehicle signature which has been extracted from the bistatic range-acquisition time map of Figure 3(a). We observe a direct signal power reduction up to 18 dB when the target crosses the baseline.

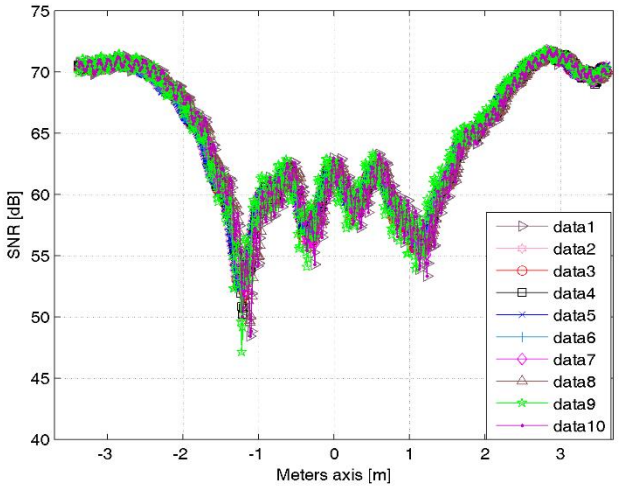

(a)

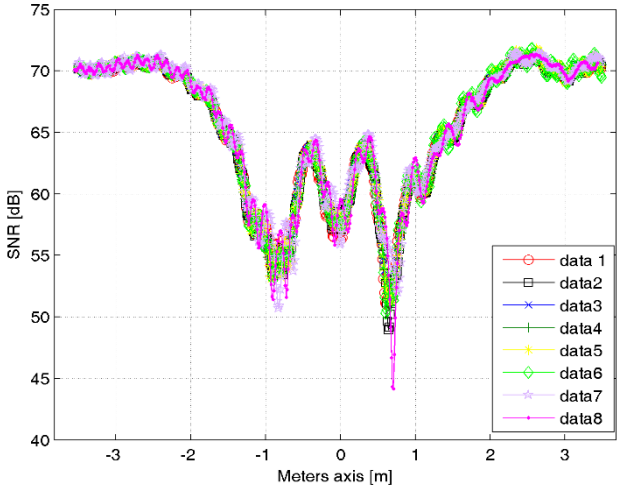

(b)

Fig. 4. Signatures comparison for the same target model on different tests. (a) Fiat Punto Evo; (b) Peugeot 107.

IV. Signature Analysis and Possible Exploitation

For a fair comparison, the vehicle signature extracted from the range compressed data cannot be used directly in a classification system because its velocity affects its shape. Therefore, a target motion estimation procedure has to be applied. Following the same strategy as in [15], in this paper, the signal after disturbance cancellation is used to estimate the component $\hat{v}$ of the target velocity orthogonal to the baseline. This estimate is then used to scale the vehicle signature from time-axis to meters-axis. This allows to directly compare (on a common axis) the signatures yield by each vehicle at different tests.

For example, Figure 4(a) reports all the signatures of the Fiat Punto Evo obtained in the performed tests. A similar shape is clearly visible for all the cases. In addition, Figure 4(b) shows the signature of the Peugeot 107 on 8 tests; we observe that also in this case, the same vehicle yields a very stable signature. Moreover, it is interesting to notice as different car models have different signature shapes. This suggests the possibility to exploit the signatures for classification purposes. In particular, a

minimum Euclidean distance criteria has been adopted to evaluate the similarity among different car models.

The adopted methodology is explained below. The target signature obtained from the k-th car model at the m-th test is collected in the vector $\underline{X}_{k,m}$ of dimensions $N \times 1$. For the considered case, $k = 1, \cdots, 4$ and $m = 1, \cdots, M_k$ where M_k is the number of the performed tests for the k-th car model (see Table I). Successively, each target signature $\underline{X}_{\overline{k},\overline{m}}$ is assumed to be the reference signature and the Euclidean distance $\eta_{k,m}^{(\overline{k},\overline{m})}$ with all the other signatures $\underline{X}_{k,m}$ is evaluated:

$$\eta_{k,m}^{(\overline{k},\overline{m})} = \frac{1}{N} \left\| \underline{X}_{\overline{k},\overline{m}} - \underline{X}_{k,m} \right\|^2 \qquad (1)$$

with $k = 1, \cdots, 4$ and $m = 1, \cdots, M_k$.

Obviously, for $\overline{k} = k$ and $\overline{m} = m$ (i.e. when the same car and number of test is considered), we obtain $\eta_{k,m}^{(\overline{k},\overline{m})} = 0$.

As is apparent, by successively varying the reference signature ($\overline{k} = 1, \cdots, 4$ and $\overline{m} = 1, \cdots, M_{\overline{k}}$) a $P \times P$ matrix of values is obtained, being $P = \sum_{k=1}^{4} M_k$, containing all the Euclidean distances evaluated for every possible pairs of tests.

V. Results against experimental data

Based on the methodology described in the previous section, the Table II shows the results obtained against the tests that employed the Peugeot 107 and the Fiat Punto Evo. Specifically the table reports the Euclidean distances (in logarithmic scale) evaluated using pairs of tests employing the same car (the Peugeot) and pairs of tests employing the two different cars. As it is apparent, the distances achieved when same car model signatures are compared are always lower than the distances achieved when different car models have been considered. Following the same criteria, Figure 5 reports in logarithmic scale the estimated distances for all the considered tests (i.e. the whole $P \times P$ matrix, being $P = 27$ in our case). Notice that the color scale dynamic range has been lower limited since zeros are obtained on the main diagonal. In particular, the first block (surrounded by a blue dashed line) and the fourth block (surrounded by a light blue dashed line) on the first block column correspond to the first and second blocks of Table II, respectively.

From the Figure 5, it is evident that the lowest values of the Euclidean distances are on the main diagonal blocks, which correspond to the tests involving the same car. Being the targets sorted in ascending order of dimensions, it is interisting to observe that the greater the difference in length among the cars, the greater the obtained distances.

For a numerical comparison, for each reference signature $\underline{X}_{\overline{k},\overline{m}}$ we report in Table III a synthesis of the results shown in Figure 5. Specifically the following strategy is adopted. The highest value is selected among results obtained with pairs of test employing the same car, namely the largest distance is reported between homologous tests. In contrast, the smallest value is reported among those obtained with pairs of tests involving a different car. Basically, the generic columns of

TABLE II. EUCLIDEAN DISTANCE VALUES ($10log_{10}\eta$) BETWEEN PEUGEOT 107 AND FIAT PUNTO EVO.

		Peugeot 107							
		1	2	3	4	5	6	7	8
Peugeot 107	1	-Inf	35,62	35,44	36,64	37,13	37,46	42,72	42,83
	2	35,63	-Inf	33,43	33,84	35,48	38,27	42,88	42,60
	3	35,44	33,43	-Inf	31,28	34,16	37,76	42,25	42,15
	4	36,64	33,84	31,28	-Inf	35,58	38,96	43,16	42,51
	5	37,13	35,48	34,17	35,58	-Inf	38,08	42,83	42,68
	6	37,46	38,26	37,77	38,95	38,06	-Inf	43,03	43,43
	7	42,73	42,88	42,25	43,15	42,83	43,04	-Inf	45,16
	8	42,82	42,53	42,14	42,46	42,68	43,37	45,16	-Inf
FIAT Punto	1	55,08	55,02	55,10	54,85	55,18	55,44	55,53	55,32
	2	55,20	55,13	55,22	54,97	55,29	55,56	55,67	55,44
	3	55,16	55,10	55,16	54,94	55,26	55,50	55,55	55,34
	4	55,20	55,13	55,21	54,97	55,30	55,55	55,61	55,39
	5	55,08	55,02	55,11	54,85	55,18	55,44	55,57	55,34
	6	54,69	54,62	54,68	54,42	54,78	55,02	55,17	54,95
	7	54,76	54,72	54,80	54,57	54,87	55,12	55,24	55,04
	8	54,89	54,84	54,91	54,66	54,97	55,20	55,37	55,17
	9	54,69	54,64	54,73	54,48	54,80	55,08	55,19	54,96
	10	54,66	54,60	54,67	54,41	54,77	55,02	55,16	54,94

Table III ($D_k^{(\overline{k},\overline{m})}, k = 1, \cdots, 4$) is based on the reference signature $\underline{X}_{\overline{k},\overline{m}}$ and is built as:

$$D_k^{(\overline{k},\overline{m})} = \begin{cases} \max\limits_{m=1,\cdots,M_k} \eta_{k,m}^{(\overline{k},\overline{m})} & for\ k = \overline{k} \\ \min\limits_{m=1,\cdots,M_k} \eta_{k,m}^{(\overline{k},\overline{m})} & for\ k \neq \overline{k} \end{cases} \qquad (2)$$

It is worth noticing that, a worst-case strategy is adopted that clearly penalizes the tests performed with identical cars. For a given target signature $\underline{X}_{\overline{k},\overline{m}}$, we conclude that the system is able to discriminate among different car signatures if the largest Euclidean distance measured among homologous tests is smaller than the smallest distance measured with any of the tests employing a different car model. If this is the case, the last row of the Table III is set to 1, otherwise is 0. Therefore:

$$\mathrm{F}^{(\overline{k},\overline{m})} = \begin{cases} 1 & if\ D_{\overline{k}}^{(\overline{k},\overline{m})} < \min\limits_{\substack{k=1,\cdots,4 \\ k\neq\overline{k}}} D_k^{(\overline{k},\overline{m})} \\ 0 & if\ D_{\overline{k}}^{(\overline{k},\overline{m})} > \min\limits_{\substack{k=1,\cdots,4 \\ k\neq\overline{k}}} D_k^{(\overline{k},\overline{m})} \end{cases} \qquad (3)$$

As it is apparent, in the majority of cases, the system is able to correctly associate the target signature to its class. Just in a single case, the Fiat Punto is confused with the Citroen C3. However, it should be pointed out that these two employed vehicles have quite similar shape and dimensions (see Table I). Nevertheless, a number of tests employing these two cars still yield correct results.

VI. Conclusions

This paper investigated the possibility to employ a passive radar in forward scatter configuration for vehicle classification.

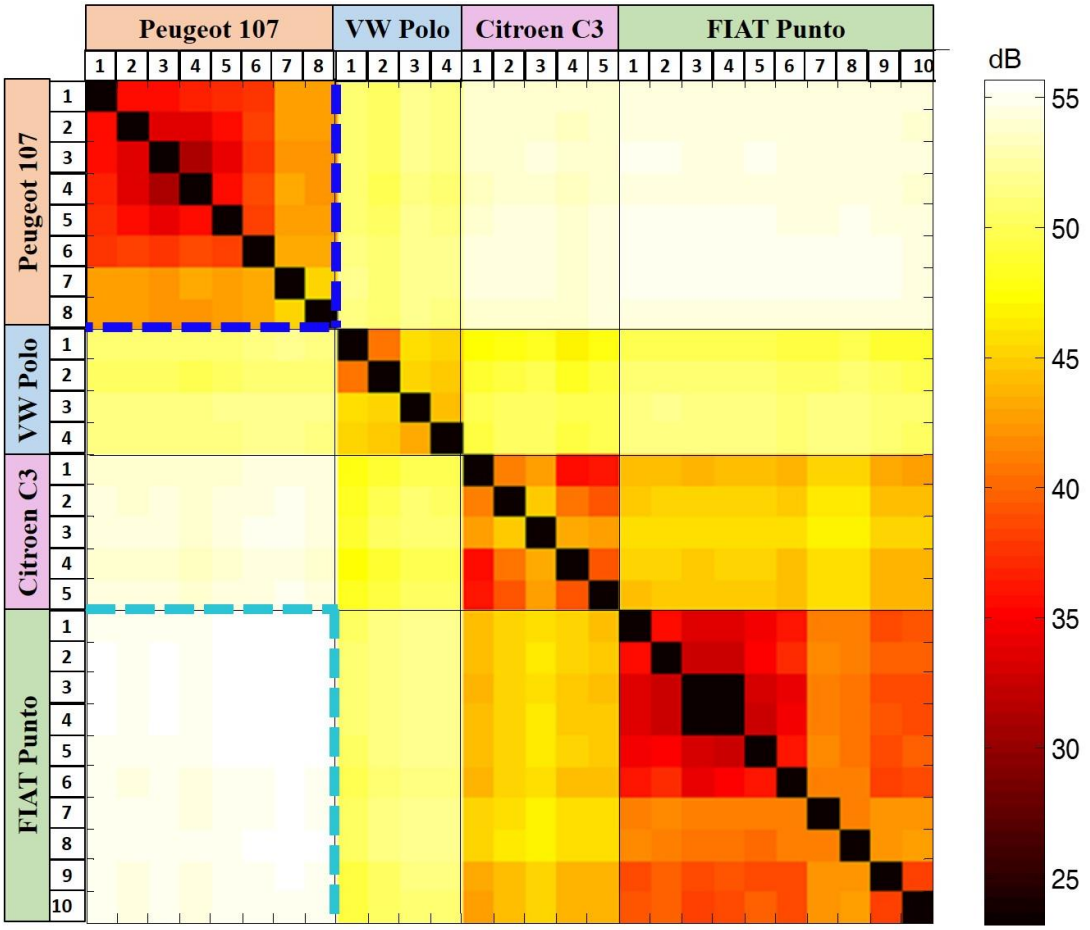

Fig. 5. Euclidean distance values for all the considered tests.

In particular, WiFi transmissions have been considered as illuminator of opportunity.

A WiFi-based PFSR system has been presented. Preliminary results against the collected data set, obtained by means of an experimental setup developed at University of Rome "La Sapienza", shown that different targets yield quite different vehicular signatures. This suggested us to exploit these signatures in a classification stage where a minimum Euclidean distance criteria has been adopted to evaluate the similarity among different car models. The results shown very good capability of the proposed system to correctly associate a vehicle signature to its car model. Therefore, the proposed system can be employed for applications of vehicle monitoring. Aiming at further investigating the potential of the WiFi-based PFSR system for vehicle classification, a more extended database including also more types of vehicle targets will have to be considered.

REFERENCES

[1] N. J. Willis, *BistaticRadar*, Tecnology Service Corporation, 1995.

[2] V. Cherniak, *Fundamentals of multisite Radar Systems*, Goldon and Breach Science Publishers, 1998.

[3] V. Sizov, M. Cheniakov and M. Antoniou, "Forward scattering radar power budget analysis for ground targets," *IET Radar, Sonar and Navigation*, 2007.

[4] M. Cherniakov, R.S.A.R. Abdullah, P. Jancovic, and V. Chapursky, "Automatic ground target classification using forward scattering radar," in *IEEE Proc. –Radar Sonar Navig.*, 2006.

[5] A.B. Blyakhman, A.V. Myakinkov, and A.G. Ryndyk, "Tracking algorithm for three-dimensional bistatic forward scattering radar with weighting of primary measurements," in *EURAD, 2005.*

[6] A.V. Myakinkov, "Optimal detection of high-velocity targets in forward scattering radar," *5th International Conference on Antenna Theory and Techniques, 2005.*

[7] H. Kabakchiev, D. Kabakchieva, M. Cherniakov, M. Gashinova, V. Behar, and I. Garvanov, "Maritime target detection, estimation and classification in Bistatic ultra wideband forward scattering radar," in *Radar Symposium (IRS)*, 2011.

[8] M. Gashinova, L. Daniel, E. Hoare, V. Sizov, K. Kabakchiev, and M. Cherniakov, "Signal characterisation and processing in the forward scatter mode of bistatic passive coherent location systems," *EURASIP Journal on Adavnces in Signal Processing*, 2013.

[9] I. Suberviola, I. Mayordomo, and J. Mendizabal, "Experimental Results of Air Target Detection With a GPS Forward-Scattering Radar," in *IEEE Geoscience and Remote Sensing Letters*, 2012.

[10] P. Krysik, K. Kulpa, and P. Samczynski, "GSM based passive receiver using forward scatter radar geometry," in *Radar Symposium (IRS), 2013.*

[11] C. Clemente, and J.J.Soraghan, "GNSS-Based Passive Bistatic Radar for Micro-Doppler Analysis of Helicopter Rotor Blades," in *IEEE Transactions on Aerospace and Electronic Systems*, 2014.

[12] M. Marra, A. De Luca, S. Hristov, L. Daniel, M. Gashinova and M. Cherniakov, "New algorithm for signal detection in passive FSR," *2015 IEEE Radar Conference*, Johannesburg, 2015.

TABLE III. SYNTHESIS OF THE RESULTS PRESENTED IN FIGURE 5 ($10log_{10}\eta$).

	Peugeot 107								VW Polo				Citroen C3					FIAT Punto								
	1	2	3	4	5	6	7	8	1	2	3	4	1	2	3	4	5	1	2	3	4	5	6	7	8	9	10
Peugeot 107	42,82	42,88	42,25	43,15	42,83	43,37	45,16	45,16	50,61	49,95	51,47	51,09	53,59	53,80	53,82	53,40	53,79	54,43	54,46	54,32	54,33	54,43	54,20	54,26	54,35	54,24	54,07
VW Polo	50,26	50,30	50,22	49,97	50,45	50,87	50,89	50,88	45,99	45,19	45,76	45,44	47,33	47,98	48,31	47,06	47,76	49,84	49,99	49,75	49,84	49,82	49,31	49,53	49,85	48,79	48,83
Citroen C3	53,74	53,65	53,72	53,39	53,78	54,17	54,34	54,04	47,34	48,66	49,77	49,70	42,62	44,87	44,97	43,15	42,93	44,19	44,30	44,01	44,20	44,45	43,59	45,29	45,29	43,18	42,69
FIAT Punto	54,66	54,60	54,67	54,41	54,77	55,02	55,16	54,94	49,17	50,23	50,86	50,92	42,71	44,40	45,31	43,72	43,67	41,52	41,54	41,14	41,29	41,40	41,19	42,32	42,76	42,22	42,60
	1	1	1	1	1	1	1	1	1	1	1	1	1	0	1	1	1	1	1	1	1	1	1	1	1	1	1

[13] F. Colone, P. Falcone, C. Bongioanni, and P. Lombardo, “WiFi-Based Passive Bistatic Radar: Data Processing Schemes and Experimental Results,” *IEEE Trans. on Aerospace and Electronic Systems*, vol. 48, no. 2, April 2012.

[14] P. Falcone, F. Colone, A. Macera, and P. Lombardo, "2D Location of Moving Targets within Local Areas using WiFi-based Multistatic Passive Radar," *IET Radar Sonar and Navigation*, vol.8, no.2, pp. 123-131, February 2014.

[15] D. Pastina, F. Colone, T. Martelli, and P. Falcone, "Parasitic Exploitation of Wi-Fi Signals for Indoor Radar Surveillance," *IEEE Trans. on Vehicular Technology*, vol.64, no. 4, April 2015.